Soft Matter

# Mechanical properties of subisostatic random networks composed of nonlinear fibers



| | |
|---|---|
| Journal: | *Soft Matter* |
| Manuscript ID | SM-ART-03-2020-000523.R2 |
| Article Type: | Paper |
| Date Submitted by the Author: | 16-Jun-2020 |
| Complete List of Authors: | Hatami-Marbini, Hamed; University of Illinois at Chicago, Mechanical & Industrial Engineering<br>Rohanifar, Milad; University of Illinois at Chicago, Mechanical and Industrial Engineering |
| | |

# Mechanical properties of subisostatic random networks composed of nonlinear fibers

Hamed Hatami-Marbini, Milad Rohanifar

*Mechanical and Industrial Engineering Department, University of Illinois at Chicago, Chicago, IL USA*

Corresponding Author:

Hamed Hatami-Marbini, PhD

2039 Engineering Research Center

843 West Taylor St

Chicago IL 60607

Email: hatami@uic.edu

Phone: 312-413-2126

# Abstract

Fibrous protein networks provide structural integrity to different biological materials such as soft tissues. These networks display an unusual exponential strain-stiffening behavior when subjected to mechanical loads. This nonlinear strain-stiffening behavior has so far been explained in terms of the network microstructure and the flexibility of constituting fibers. Here, we conduct a comprehensive computational study to characterize the importance of material properties of individual fibers in the overall nonlinear mechanical response of random fiber networks. To this end, we consider three nonlinear material models, ranging from an almost linear form to a highly nonlinear one, for the fibers of subisostatic disordered networks. We characterize the amount of strain-stiffening as a function of bending rigidity of the fibers, the amount of nonlinearity of the fibers, and the connectivity of random networks. We find that networks composed of highly nonlinear fibers exhibit much more strain-stiffening than networks made up of linear fibers. Furthermore, the local strain distribution becomes more homogenous as the amount of nonlinearity in material models increases. Increasing the network connectivity signifies the importance of the nonlinear material response of fibers in the overall mechanical behavior of networks. The constitutive behavior of fibers plays an important role in defining the failure response of networks particularly in the damage initiation and evolution. The findings of this work show how the mechanical response of individual fibers affects the overall mechanical properties of random networks and could find applications in designing new biomimetic materials and better understanding of the mechanical properties of biological materials.

# Introduction

The mechanical properties of the cytoskeleton and extracellular matrix play a crucial role in the cellular shape and function [1]. The extracellular matrix is a network of different macromolecules such as collagen fibers and proteoglycans. The collagen, the primary load-bearing constituent within the extracellular matrix, is the most abundant fibrous protein and is commonly found in tissues such as articular cartilage, ligaments, cornea, and tendons [2, 3]. Similarly, cytoskeleton is a composite network of protein fibers that gives structural integrity to cells [4, 5]. This fibrous network participates in numerous vital processes such as cell motility, apoptosis, and division [6]. It is challenging to develop a complete understanding of the nonlinear mechanics of fibrous networks.

Previous experimental studies reveal that biopolymer networks exhibit nonlinear elasticity and can undergo large deformation [7-10]. The distinct feature of biopolymers such as those found in the cell cytoskeleton and extracellular matrix of tissues is their finite bending rigidity. There are many numerical and theoretical efforts in the literature to explain the mechanics of these semiflexible fiber networks in terms of elastic properties of their individual fibers and network architecture [10-12]. In affine models, fiber segments are assumed to deform according to the applied far-field strain; thus, the macroscopic mechanical response of networks can be expressed in terms of a number of microstructural parameters such as the fiber orientation and crosslinking density [7, 8]. However, the mechanical response of fiber networks, especially those that are found in biological world, is nonaffine [13-17].

Affine and nonaffine numerical models using both lattice-based and off-lattice network structures have been used to investigate the origins of the nonlinear elasticity of fibrous networks [10-12, 18-24]. It is concluded that random networks display soft mechanical response at small strains, primarily

governed by soft bending deformation of the fibers. However, they show strong nonlinear strain-stiffening behavior with more affine deformation at large strains [7, 8, 22, 25, 26]. The importance of hierarchical and complex microstructure of these networks in their remarkable mechanical properties under finite deformation has well been recognized [7, 22, 27-34]. In particular, considerable attention has been given to the network connectivity, network architecture, and type of disorders. However, lesser attention has been directed towards the potential role that the nonlinear mechanical response of constituting fibers could play in controlling the elasticity of random networks.

The primary objective of the present study is to elaborate on the influence of material nonlinearity of individual fibers on the mechanical behavior of random networks. This investigation uses an exponential function to express the stress-strain response of the fibers. The amount of nonlinearity is varied from low to high and the numerical findings are compared with previous studies that utilized the linear elastic model for fibers. The microstructure of networks in numerical simulations is represented by diluted triangular lattices with different connectivity. The mechanical response of fibrous networks is only studied under shear but similar response is expected in other modes of deformation. The effect of bending rigidity of fibers and its relation to the nonlinearity of the network mechanical response are also characterized. The maximum strain in fiber segments is calculated as a function of applied deformation in order to determine the local strain distribution throughout the networks. The influence of constitutive models of fibers on the failure response is also studied by considering a strain-based failure criterion. Both the onset and the evolution of damage in the networks are characterized. The numerical results show that the mechanical response of constituting fibers has important effects on the mechanical properties of random polymer networks.

## Numerical Model:

Biopolymers usually form crosslinked network structures with an average connectivity z between 3 and 4 at crosslinks [20, 35]. Thus, the bending of fibers, in addition to their axial elasticity, is required for stabilizing these subisostatic and unstable networks [12, 31]. Herein, we only consider subisostatic networks made up of athermal fibers that are modelled as beam elements, i.e. the mechanical behavior is only studied under pure enthalpic contributions and possible effects of thermal bending fluctuations are not considered.

We only consider two-dimensional (2D) random diluted triangular networks. The fibers are first arranged into triangular lattice of size WxW and fiber segments of equal length $l$ are assumed to be permanently crosslinked at the vertices[36]. The resulting networks have a connectivity of z = 6; thus, we randomly remove fiber segments with a probability of 1 – p until the connectivity becomes less than the 2D isostatic threshold, z = 4, Figure 1 [20]. Any remaining dangling ends are removed and the average coordination number of lattice-based networks is calculated. Unless otherwise stated, the average connectivity is kept between 3 and 4 in order to obtain networks compatible with what typically seen in biological materials [31]. All simulations are performed using networks of size W = 50$l$ in order to minimize the possible effects of the size of networks [21]. The representative data is shown; however, it is confirmed that no significant variation exists in the data obtained from at least five network realizations.

The fiber stands are modeled as nonlinear Timoshenko beams taking into account their stretching, shear, and bending deformations. For networks composed of linear elastic fibers, the beam segments are assumed to have cross-sectional area A, second moment of inertia I, Young's modulus E, stretching modulus $\mu$ = EA, and bending rigidity $\kappa$ = EI, and thus, dimensionless

bending rigidity $\bar{\kappa} = \kappa / \mu l^2$. The dimensionless bending rigidity quantifies the flexibility of the fibers and is varied from 0.00001 to 0.1 in the present study. In order to investigate the effect of nonlinear constitutive behavior of fibers on the mechanical response of random networks, we also consider fibers whose constitutive law is nonlinear. To this end, we assume that fibers have an initial linear elastic response followed by an exponential hardening response [37], i.e.

$$\sigma_f = \begin{cases} E\varepsilon & \varepsilon \le \varepsilon_Y \\ EB\left(e^{(\varepsilon-\varepsilon_Y)/B} - 1\right) + E\varepsilon_Y & \varepsilon > \varepsilon_Y \end{cases} \qquad (1)$$

where $\varepsilon_Y$ denotes the strain at which the linear elastic behavior switches to an exponential form, and B is a material constant that controls the amount of nonlinearity. B is varied between 1 (Model I: slightly nonlinear), 0.2 (Model II: nonlinear), and 0.1 (Model III: highly nonlinear) in this work, Figure 1b. The commercial software ABAQUS is used to conduct the numerical simulations using both static and implicit finite element methods. The fiber segments are divided into smaller elements in order to capture their nonlinear bending accurately. A user-defined material (UMAT) is written to represent the nonlinear stress-strain response of nonlinear fibers in ABAQUS. A high-performance computing cluster is used to solve for the mechanical response of diluted triangular lattice networks subjected to large shear deformation.

In order to apply the shear strain $\gamma$, all fibers intersecting the lower horizontal boundary are only fixed in the horizontal and vertical directions, and those attaching to the upper horizontal boundary are constrained to translate horizontally. The finite shear strain $\gamma$ is applied incrementally and no constraint is defined for the fibers intersecting the vertical boundaries of the domain. The shear strain is applied incrementally in 100 steps from 0 to 100%. Static analysis is used for shear strains upto 30% - 40% and implicit static method is used for finding the deformation at larger strains. It

is ensured that the ratio of kinetic energy and elastic energy to be very small in the implicit analysis. Once the finite element simulation results are obtained, we calculate the shear stress by dividing the summation of forces in the fibers intersecting the upper lattice boundary by W [38]. The differential shear modulus of the networks, also referred to as stiffness herein, at each increment is defined as the slope of the stress-strain response, i.e. $K = \partial\sigma/\partial\gamma$, where $\gamma$ and $\sigma$ are the applied shear strain and calculated shear stress, respectively. In the following, the stress and stiffness are given in units of $\mu/l$.

**Figure 1**

**Fig. 1** a) The microstructure of disordered fiber networks is represented by diluted triangular lattices b) The normalized stress-strain response of fibers; the parameter B determines the amount of nonlinearity and the constitutive relation, eq. (1), is defined such that the fibers show an initial linear elastic response in all models.

## Results and Discussion

It has been shown that random fibrous networks exhibit remarkable strain-stiffening when subjected to large shear deformation [22, 27]. This means that the shear stiffness of these networks significantly increases with the strain. This stiffening behavior mainly depends on the fiber bending rigidity and the connectivity of random networks. Previous studies examined the role of connectivity on the mechanism of deformation (bending versus stretching dominated behavior) [15, 31, 34, 39]. The disordered fiber networks with connectivity above the central-force isostatic point are more likely to show stretching dominated behavior. In contrast, subisostatic networks, typically seen in the biological world, are floppy and often depict bending dominated response (note that

fibers with large bending rigidity cause stretching dominated response even in subisostatic networks[10, 14, 15]).

The mechanical response of networks composed of linear elastic fibers can be divided into three regimes depending on the applied strain (Figure S1). When the applied shear strain is smaller than the critical value $\gamma_0$, an almost constant shear rigidity K, i.e. $\sigma \propto \gamma$, is seen independent of $\bar{\kappa}$. In this regime, the dominant deformation mechanism is fiber bending and $K \propto \bar{\kappa}$. The critical strain $\gamma_0$ denotes the onset of nonlinearity in the overall mechanical response. Similar to previous studies [20, 22], we observe that $\gamma_0$ is almost independent of $\bar{\kappa}$ for networks composed of linear elastic fibers. With increasing the applied shear strain ($\gamma > \gamma_0$), the strain-stiffening response proceeds in two consecutive steps. During the first stage, the shear stress and differential shear modulus increase nonlinearly upto the point when the applied shear strain reaches a second critical value $\gamma_c$, denoted by star symbols in Figure S1. At this critical strain, the stretching deformation of the fibers becomes the dominant mode of deformation and the network rigidity becomes independent of $\bar{\kappa}$. The critical shear strain $\gamma_c$ is defined as the strain at which an inflection point appears in log(K) versus log($\gamma$) [20, 21]. Figure S1 shows that $\gamma_c \sim$ 45-55% and is weakly dependent on the bending rigidity of the fibers. The critical strain can also be estimated from the ratio of relative contributions of bending and stretching energy to the total elastic energy. For strains larger than $\gamma_c$, the total energy is dominated by fiber stretching, Figure S2. The fibers of biological materials behave nonlinearly especially if the mechanical response under large deformation is of interest. Thus, it is important to investigate whether the above observations hold when random networks composed of nonlinear fibers, eq. (1), are considered.

***Effect of nonlinear stress-strain behavior of fibers on the network shear modulus:***

Figures 2 a-b plot the normalized shear stiffness of networks composed of nonlinear fibers with $\bar{\kappa}$ = 0.01 and $\bar{\kappa}$ = 0.00001 as a function of normalized shear strain. In these plots, the shear stiffness K is normalized with the stiffness of similar networks composed of linear elastic fibers, Figure S1. Furthermore, the applied shear strain is normalized by $\gamma_d$, which is the far-field shear strain at which the strain in at least one of the fiber segments reaches the yielding strain $\varepsilon_Y$, eq. (1). The plots shown as the insets of Figures 2a-b confirm that the variation of network stiffness with the applied shear strain upto $\gamma_d$ is similar to what is observed for networks of linear elastic fibers (Figure S1); this is because all fibers (even nonlinear ones) are assumed to have the same linear elastic material response, eq. (1), initially. Figure 2c plots the variation of critical shear strain $\gamma_d$ as a function of $\bar{\kappa}$; this plot shows that this parameter has an inverse relation with the bending rigidity of fibers. In particular, $\gamma_d \propto \bar{\kappa}^{-0.5}$. The variation of the initial shear modulus at $\gamma \sim 1\%$, denoted by G, as a function of $\bar{\kappa}$ is also shown in the inset of Figure 2c. It is seen that $G \propto \bar{\kappa}$, i.e. a bending dominated regime exists and the initial modulus is proportional to $\bar{\kappa}$ [14]. The flexibility of fibers, characterized by $\bar{\kappa}$, determines their local strain, as discussed later in this work.

Figure 2a shows the mechanical response of networks composed of fibers with relatively large bending rigidity ($\bar{\kappa}$ = 0.01). These fibers could not accommodate the applied deformation by rigid rotations and their internal energy increases due to the applied shear strain such that their local strain reaches the yielding point $\varepsilon_Y$ defined in the constitutive relation (1). Thus, they exhibit nonlinear mechanical response and the mechanical properties of their respective disordered networks become distinct from those of networks composed of only linear elastic fibers. It is

interesting to note that $\gamma_d$ for networks composed of stiff fibers (large $\bar{\kappa} \sim 0.01$) is close to and might even be less than $\gamma_0$ (the linear regime shown in Figure S1). When $\gamma < \gamma_d$ in these networks, the role of material properties of individual fibers is insignificant and bending deformation dominates their overall shear response. With increasing the applied shear strain, a nonlinear stiffening regime followed by a linear stiffening regime is observed.

The critical strain $\gamma_d$ for networks composed of flexible fibers (small $\bar{\kappa} \sim 10^{-5}$) is significantly larger than $\gamma_0$ and occurs at strains closer to the critical shear strain $\gamma_c$, see the inset of Figure 2b which is plotted for networks with $\bar{\kappa} = 0.00001$. Note that $\gamma_d \sim 35\%$ and $\gamma_c \sim 47\%$ for these networks, Figure 2c and Figure 2f. Thus, the effect of the material nonlinearity of fibers is only observed after their complete reorientation in the loading direction, where the networks enter the stretching dominated regime. This can be easily seen by plotting the relative contributions of bending and stretching energy, Figure 2f.

For applied shear strains larger than $\gamma_d$ (i.e. $\gamma/\gamma_d > 1$) and independent of $\bar{\kappa}$, networks of nonlinear fibers exhibit a significant higher stiffening when compared to networks with linear elastic fibers, Figures 2a-b; this stiffening is a function of both the applied strain and the intensity of nonlinear response of individual fibers. For example, the stiffness of networks composed of Model III fibers with $\bar{\kappa} = 0.00001$ at $\gamma = 100\% >> \gamma_d$ becomes seven-fold larger than that of similar networks made up of linear elastic fibers. Figure 2d plots the variation of stiffness as a function of $\bar{\kappa}$ at $\gamma = 60\%$ and 100% for networks composed linear and nonlinear fibers (note that $\gamma_d < 60\%$ for all models). Although the difference between various material models at $\gamma = 1000\%$ is significant and almost independent of the bending rigidity of fibers, the difference between various material models is

relatively small at $\gamma$ = 60% and slightly varies with $\bar{\kappa}$. This is because the stretching of fibers is dominant at large applied shear strains ~ 100%. At smaller strains ~ 60%, the influence of material models becomes slightly more marked with increasing the bending rigidity of fibers. This is because increasing $\bar{\kappa}$ enhances the role of fiber stretching in the deformation mechanism resisting the external deformation[15, 16, 20, 39]. Figures 2e-f show that the interrelation between $\bar{\kappa}$ and the nonlinearity of fibers determines the bending- versus stretching-dominated behavior in random networks.

The results so far suggest that networks with nonlinear fibers exhibit distinctly different response when compared to the behavior of those composed of linear fibers when the applied strain becomes large. The bending rigidity of constituting fibers, defined by $\bar{\kappa}$, is a fundamental factor determining the value of applied strain, $\gamma_d$, at which the nonlinearity of individual fibers shows its effect on the overall network mechanical properties. Furthermore, the nonlinear intensity of constitutive response of fibers is another important factor affecting the rate of strain stiffening.

**Figure 2**

**Fig. 2** The effect of nonlinear elastic properties of individual fibers on the mechanical response of fibrous networks. The normalized network stiffness, $K/K_{linear}$, as a function of the normalized applied shear strain $\gamma/\gamma_d > 1$ for a) $\bar{\kappa} = 10^{-2}$ and b) $\bar{\kappa} = 10^{-5}$. The insets show the variation of the network stiffness K versus the applied shear strain c) The variation of $\gamma_d$ versus the dimensionless bending rigidity $\bar{\kappa}$; the linear modulus $G_0$ at $\gamma$ = 1% is plotted as a function of $\bar{\kappa}$ in the inset. d) The network stiffness K is plotted as a function of $\bar{\kappa}$ at shear strains $\gamma$ = 60% and $\gamma$ = 100%. The effect of material nonlinearity of fibers is more pronounced when the applied shear strain increases and when the bending rigidity of fibers increases. The relative contributions of stretching energy $H_s$ and bending energy $H_b$ versus the applied shear strain for e) $\bar{\kappa} = 10^{-2}$ and f) $\bar{\kappa} = 10^{-5}$; $H = H_s + H_b$. The critical shear strain $\gamma_c$ is a function of bending rigidity of the fibers and a significant difference between the linear and nonlinear network especially for $\gamma > \gamma_c$.

Another interesting feature of fibrous networks is the nonlinear increasing of their differential shear modulus K as a function of the shear stress σ. The networks of linear elastic fibers stiffen as $K \propto \sigma^{\alpha}$ where α depends on the bending rigidity of fibers and varies from about 1.5 ($\bar{\kappa}$ = 0.00001) to 0.6 ($\bar{\kappa}$ = 0.1), see Figure S3. These findings agree with previous numerical, experimental, and theoretical reports that show that the exponent increases from 0.5 to 1.5 with decreasing $\bar{\kappa}$ for networks composed of linear elastic fibers [20, 22, 40]. However, we do not observe a unique exponent of 1.5 in the initial stiffening regime that has been reported from computer simulations of a random network comprised of cross-linked biopolymer-like fibers [11, 24]. We also observe that the range of the initial stiffening becomes smaller with increasing $\bar{\kappa}$, Figure S3. Finally, at very large shear stresses (and in agreement to what has been previously reported [20, 22, 40]), the stress-stiffening response of linear elastic fiber networks vanishes, which disagrees with experimental measurements where the network stiffness increases until failure [22]. With increasing the shear stress, the deformation of networks becomes stretching dominated (Figure 2e-f) and the nonlinearity of fibers causes the overall response of the networks to be nonlinear; numerical models using linear elastic fibers could not capture this important phenomenon.

The material nonlinearity of fibers does not significantly affect the initial stress-stiffening behavior of networks especially when $\bar{\kappa}$ is very small. However, with increasing the bending rigidity of fibers, the difference between numerical models composed of linear and nonlinear fibers becomes more pronounced, Figure 3 and Figure S3. It is interesting to note that numerical models with linear elastic fibers may introduce errors in the estimates of α at large stress values (shown pictorially by dashed lines in Figure S3). The present results, that are obtained using fibers with different levels of nonlinearity, suggest that the stiffening exponent at large shear stresses is a function of nonlinear behavior of the fibers.

Figure 3 shows that the stress-stiffening, $K \propto \sigma^{\alpha}$, proceeds in three regimes. Initially $\alpha \sim 0$ for all $\bar{\kappa}$'s ($\gamma < \gamma_0$), $\alpha$ then varies from about 0.6 to 1.5 depending on $\bar{\kappa}$ as the applied load increases ($\gamma > \gamma_0$), and $\alpha$ finally becomes about 1.0 for all $\bar{\kappa}$'s at large shear stresses ($\gamma >> \gamma_0$). It is observed that increasing the nonlinearity of fibers makes the stress-stiffening curve depicts a single exponent, i.e. the shape of the stiffness-stress curve becomes similar to mechanical response of collagenous tissues.

**Figure 3**

**Fig. 3** The variation of the differential shear modulus of nonlinear fiber networks versus the shear stress. The results are shown for Model III fibers and $\bar{\kappa} =$ 0.00001-0.1. Three different regions are observed. Initially, the network stiffness is independent of the stress. With increasing the stress, the stiffness increases as $K \sim \sigma^{\alpha}$ where $\alpha$ varies from 0.6 to 1.5 as $\bar{\kappa}$ decreases from $10^{-1}$ to $10^{-5}$ (the inset). With further increase of the stress, the stiffness increases as $K \sim \sigma^{\alpha}$ where $\alpha \sim 1$. The shear modulus and stress are plotted in units of $\mu/l$.

***Effect of nonlinear stress-strain behavior of fibers on local strain distribution:***

Next, we investigate the local strain distribution as a function of the applied shear strain in both linear and nonlinear fiber network models, Figure 4. No significant difference is observed between different numerical models when the applied shear strain $\gamma$ is less than $\gamma_d$. However, a distinct response is found for each model as $\gamma > \gamma_d$. There is an almost linear relation between the macroscopic shear strain $\gamma$ and the maximum local strain $\varepsilon_{max}$ for networks composed of linear elastic fibers. On the other hand, increasing the nonlinearity in fibers reduces the maximum local strain. As shown in Figure 4a, $\varepsilon_{max}$ has its lowest value for networks composed of fibers with

material Model III. It is also noted that increasing the applied shear strain causes the difference between maximum local strains for different models becomes more significant. Compared to models with linear fibers, the maximum local strain, at $\gamma = 100\%$, in those with fibers with material Models II and III decreases nearly 40% and 60%, respectively.

In order to have a better understanding of local strain distribution, we characterize the distribution of the local strain $\varepsilon_l$ in all fiber segments when the applied shear strain $\gamma$ is 100%. The strain $\varepsilon_l$ in different simulations are normalized by the respective maximum local strain $\varepsilon_{max}$ and are reported as $R = |\varepsilon_l / \varepsilon_{max}|$ where the symbol | | represents absolute value. As depicted in Figure 4b, the mechanical response of individual fibers has a substantial influence on the local strain distribution. In models with linear elastic fibers, the majority of segments, i.e. about 97% of them, takes small strains ($R < 0.4$), nearly 2.5% of segments takes medium strains ($0.4 < R < 0.6$), and only less than 0.5% takes very large local strains ($R > 0.6$). In other words, there is a significantly large unbalance between the numbers of elements with high and low strains. As the nonlinearity in the material behavior of fibers increases, the number of fibers with higher local strain shows a significant increase, i.e. about 72%, 20%, and 8% of fiber segments following material Model III have small ($R < 0.4$), medium ($0.4 < R < 0.6$), and large ($R > 0.6$) local strains, respectively. This observation is an indication of a more uniform strain distribution in networks composed of nonlinear fibers. The uniformity of local strain distribution is a crucial factor in defining the damage response of fiber networks. While fibers with high local strains define the damage onset, the strain distribution inside the domain determines how the damage progresses.

**Figure 4**

**Fig 4** a) The maximum local strain in individual fibers as a function of the applied shear strain for networks composed of fibers with linear and nonlinear mechanical response and $\bar{\kappa} = 10^{-2}$. b) The probability distribution function of the local strain magnitude when the applied shear is $\gamma = 100\%$.

***Effect of network connectivity on mechanical response of nonlinear fiber networks***

The numerical simulations have so far been obtained from fiber networks with an average connectivity of about 3.10. It is known that the average connectivity plays an important role in defining the mechanical response of random fiber networks [29, 31, 41]. In the following, we briefly investigate the effects of material behavior of individual fibers on the mechanical properties of networks with various connectivity. We leave a more complete study of this topic for a future study and only consider networks with $3 < z < 4$ (consistent with what typically found in biopolymer networks).

Figure 5 plots the shear modulus as a function of the applied shear strain for networks with various connectivity in order to show the effect of the nonlinear response of fibers. Increasing z enhances the effect of the material nonlinearity of fibers on the network stiffness even for those composed of fiber with very low $\bar{\kappa}$, Figure 5a. Furthermore, increasing z causes $\gamma_d$ to shift towards smaller strains, which means that fibers reach their yielding strain at smaller applied shear strain. Previous studies on the mechanical response of linear random networks show that both the network connectivity and the bending rigidity of fibers determine the dominant mode of deformation during initial stages of shearing ($\gamma < \gamma_0$) [14, 15]. With increasing the bending rigidity of fibers, the dominant mode of deformation switches from bending to stretching even for networks with low network connectivity. In particular, $\gamma_d$ shows small variations with z at $\bar{\kappa} = 0.01$, Figure 5b. For these

networks, the far-field shear strain causes the fibers to deform in stretching mode and to reach their yielding strain at about 2-5% independent of z.

The average connectivity also affects the stiffening rate of random networks. As discussed before, networks composed of nonlinear fibers exhibit stiffer response compared to those with linear elastic fibers. To quantify the stiffening as a function of network connectivity, we plot the ratio of maximum shear moduli obtained using Model III and linear elastic model in Figure 5c. The stiffness of networks composed of Model III fibers is 5-fold and 17-fold higher than that of the similar networks with linear fibers for z = 3 and z = 3.84, respectively. Figure 5c shows that bending rigidity of fibers has little effects on this ratio. This is because the dominant mode of deformation at very large shear strain of 100% is stretching.

**Figure 5**

**Fig 5** The effect of the nonlinear response of fibers on the mechanical properties of random fiber networks with various average connectivity a) The shear modulus K is plotted as a function of the applied shear strain for networks composed of linear and Model III fibers when $\bar{\kappa} = 10^{-4}$. b) The variation of $\gamma_d$ as a function of network connectivity z is shown for networks with $\bar{\kappa} = 10^{-2}$ and $\bar{\kappa} = 10^{-4}$. c) The ratio of differential moduli at $\gamma = 100\%$ for networks composed of nonlinear fibers (Model III) and those with linear fibers is plotted as a function of network connectivity when $\bar{\kappa} = 10^{-2}$ and $\bar{\kappa} = 10^{-4}$.

***Effect of nonlinear stress-strain behavior of fibers on failure response of random networks***

In the last section of the present study, we briefly investigate the effects of fiber material nonlinearity on the failure response of random networks. The fracture behavior of disordered fiber networks is a complex problem because of the non-uniform distribution of defects, which creates stress concentration with different intensities throughout the simulation domain. Since the roles of

network connectivity and flexibility of fibers in the fracture process have recently been studied [42], we primarily explore the effects of the nonlinear response of fibers. For this purpose, we consider subisostatic networks with fixed connectivity $z \sim 3.1$ under shear strain. The shear strain is applied incrementally and possible stress/strain redistribution associated with the failure of fibers is quantified at each step. The incremental strain is selected such that the successional appearance and disappearance of force chains could be captured throughout the failure process. Here, we use a strain-based failure criterion in which fiber segments are removed when their maximum strain reaches the failure strain $\varepsilon_f^{max} = 0.325$. The applied shear strain is increased until networks break into two separate pieces. Figure 6 shows the force-displacement curve related to step-wise damage process of fiber networks with $\bar{\kappa} = 0.06$ and $\bar{\kappa} = 0.001$. It is seen that regardless of the material model of fibers and their bending rigidity, the onset of damage occurs in the strain stiffening regime ($\gamma > \gamma_0$). In other words, with increasing the applied shear deformation, a few primary force chains appear in networks. These force chains continue to carry the applied load until a fiber segment along them fails. Upon further shearing of the networks, new primary force chains emerge. The appearance and disappearance of force chains, causing the stress redistribution, continue until the final failure. With increasing the material nonlinearity of fibers, the damage onset and complete failure shift to larger applied shear strain. This is because nonlinear fibers create more homogeneous local strain distribution throughout the network microstructure (see Figure 4); thus, more fiber segments contribute to the overall strength of fiber networks. With increasing the rigidity of linear fibers, the failure behavior of networks become more brittle, i.e. a single crack in a serrated pattern will lead to the final failure of the structure, Figure 6c. On the other hand, diffusive form of failure dominates networks composed of nonlinear fibers, Figure 6d. A diffusive failure occurs when fiber segments fail at (and are subsequently removed from)

different locations in networks; this failure pattern is observed when local strain distribution is homogenous. In this failure pattern, there exists a notable lag between the damage onset and the final failure of the networks; this lag is proportional to the nonlinearity of the fibers, Figure 6e. Keeping the bending rigidity constant and increasing the nonlinearity of fibers' mechanical behavior result in a more diffusive form of damage propagation, Figure 6. The bending rigidity of fibers directly influences the diffusive crack propagation rate in networks composed nonlinear fibers. The distinct damage locations and stress redistribution are primary factors causing the appearance of fluctuation in the force-displacement curves. Accordingly, more fluctuation is observed between the onset and final failure of networks with nonlinear fibers; this phenomenon is more obvious in networks composed of more flexible fibers.

**Figure 6**

**Fig. 6** The effects of material nonlinearity of individual fibers on the shear stress-strain curves for networks with a) $\bar{\kappa}$ = 0.06 b) $\bar{\kappa}$ = 0.001. The influence of material properties of individual fibers on the damage propagation pattern is also shown for networks at $\bar{\kappa}$ = 0.06; c) a single crack is formed and expands for networks composed of linear elastic fibers while d) multiple cracks are formed and expand throughout networks of nonlinear fibers (material Model III) e) The effect of material nonlinearity of fibers on the lag between the onset ($\gamma = \gamma_0$) and the complete ($\gamma = \gamma_f$) failure of random networks composed of fibers with different bending rigidity.

## Conclusion

The present study characterizes the effects of material properties of individual fibers on the mechanical response of random networks with nonlinear fibers. Different material models ranging from an almost linear elastic model to nonlinear constitutive models are considered for the

mechanical response of fibers. The nonlinear behavior of fibers is represented by an exponential material model such that the amount of nonlinearity could be tuned in different numerical simulations. All networks show initially a linear stress-strain response upto a critical strain $\gamma_0$. In networks composed of nonlinear fibers, with further increase of the applied shear strain, strain in fiber segments increases and the linear elastic behavior switches to an exponential form when the local strain reaches $\varepsilon_Y$. The applied shear strain at which at least one of the fibers reaches strain $\varepsilon_Y$ is represented by $\gamma_d$, this strain depends on the bending rigidity of fibers. A significant strain-stiffening is observed with increasing the applied shear strain beyond $\gamma_d$. The networks of nonlinear fibers exhibit stronger stiffening as a function of applied strain; the amount of this stiffening is directly proportional to the intensity of the nonlinearity of fibers. The material properties of fibers have a direct influence on the local strain distribution inside the networks. The local strains tend to have a more homogenous and uniform distribution in networks of nonlinear fibers. The network connectivity plays a significant role in the way that the material nonlinearity of individual fibers influences the overall elasticity of random networks. The networks with higher connectivity are more sensitive to the material properties of fibers; decreasing the flexibility of fibers intensifies this effect. The nonlinearity of fibers also changes the failure response of random networks. In particular, compared to networks of linear fibers, the damage propagation becomes more diffusive in networks with nonlinear fibers.

## Acknowledgements:

The authors would like to acknowledge the support in part by National Science Foundation: Grant No. 1636659.

# Figure captions

**Figure 1** a) The microstructure of disordered fiber networks is represented by diluted triangular lattices b) The normalized stress-strain response of fibers; the parameter B determines the amount of nonlinearity and the constitutive relation, eq. (1), is defined such that the fibers show an initial linear elastic response in all models.

**Figure 2** The effect of nonlinear elastic properties of individual fibers on the mechanical response of fibrous networks. The normalized network stiffness, $K/K_{linear}$, as a function of the normalized applied shear strain $\gamma/\gamma_d > 1$ for a) $\bar{\kappa} = 10^{-2}$ and b) $\bar{\kappa} = 10^{-5}$. The insets show the variation of the network stiffness K versus the applied shear strain c) The variation of $\gamma_d$ versus the dimensionless bending rigidity $\bar{\kappa}$; the linear modulus $G_0$ at $\gamma = 1\%$ is plotted as a function of $\bar{\kappa}$ in the inset. d) The network stiffness K is plotted as a function of $\bar{\kappa}$ at shear strains $\gamma = 60\%$ and $\gamma = 100\%$. The effect of material nonlinearity of fibers is more pronounced when the applied shear strain increases and when the bending rigidity of fibers increases. The relative contributions of stretching energy $H_s$ and bending energy $H_b$ versus the applied shear strain for e) $\bar{\kappa} = 10^{-2}$ and f) $\bar{\kappa} = 10^{-5}$; $H = H_s + H_b$. The critical shear strain $\gamma_c$ is a function of bending rigidity of the fibers and a significant difference between the linear and nonlinear network especially for $\gamma > \gamma_c$.

**Figure 3** The variation of the differential shear modulus of nonlinear fiber networks versus the shear stress. The results are shown for Model III fibers and $\bar{\kappa} =$ 0.00001-0.1.Three different regions are observed. Initially, the network stiffness is independent of the stress. With increasing the stress, the stiffness increases as $K \sim \sigma^{\alpha}$ where $\alpha$ varies from 0.6 to 1.5 as $\bar{\kappa}$ decreases from $10^{-1}$ to $10^{-5}$ (the inset). With further increase of the stress, the stiffness increases as $K \sim \sigma^{\alpha}$ where $\alpha \sim 1$. The shear modulus and stress are plotted in units of $\mu/l$.

**Figure 4** a) The maximum local strain in individual fibers as a function of the applied shear strain for networks composed of fibers with linear and nonlinear mechanical response and $\bar{\kappa} = 10^{-2}$. b) The probability distribution function of the local strain magnitude when the applied shear is $\gamma$ = 100%.

**Figure 5** The effect of the nonlinear response of fibers on the mechanical properties of random fiber networks with various average connectivity a) The shear modulus K is plotted as a function of the applied shear strain for networks composed of linear and Model III fibers when $\bar{\kappa} = 10^{-4}$. b) The variation of $\gamma_d$ as a function of network connectivity z is shown for networks with $\bar{\kappa} = 10^{-2}$ and $\bar{\kappa} = 10^{-4}$. c) The ratio of differential moduli at $\gamma$ = 100% for networks composed of nonlinear fibers (Model III) and those with linear fibers is plotted as a function of network connectivity when $\bar{\kappa} = 10^{-2}$ and $\bar{\kappa} = 10^{-4}$.

**Figure 6** The effects of material nonlinearity of individual fibers on the shear stress-strain curves for networks with a) $\bar{\kappa}$ = 0.06 b) $\bar{\kappa}$ = 0.001. The influence of material properties of individual fibers on the damage propagation pattern is also shown for networks at $\bar{\kappa}$ = 0.06; c) a single crack is formed and expands for networks composed of linear elastic fibers while d) multiple cracks are formed and expand throughout networks of nonlinear fibers (material Model III) e) The effect of material nonlinearity of fibers on the lag between the onset ($\gamma = \gamma_0$) and the complete ($\gamma = \gamma_f$) failure of random networks composed of fibers with different bending rigidity.

# References


1. K. Bhadriraju and L. K. Hansen, *Experimental Cell Research*, 2002, **278**, 92-100.
2. H. Lodish, A. Berk, C. A. Kaiser, M. Krieger, M. P. Scott, A. Bretscher, H. Ploegh and P. Matsudaira, *Molecular cell biology*, Macmillan, 2008.
3. H. Hatami-Marbini and E. Etebu, *Experimental eye research*, 2013, **116**, 47-54.
4. H. Hatami-Marbini and M. R. Mofrad, in *Complex Fluids in Biological Systems*, Springer, 2015, pp. 187-205.
5. H. Hatami-Marbini and M. R. Mofrad, in *Cellular and biomolecular mechanics and mechanobiology*, Springer, 2010, pp. 3-27.
6. T. D. Pollard, *Journal of supramolecular structure*, 1976, **5**, 317-334.
7. F. C. MacKintosh, J. Käs and P. A. Janmey, *Phys Rev Lett*, 1995, **75**, 4425-4428.
8. C. Storm, J. J. Pastore, F. C. MacKintosh, T. C. Lubensky and P. A. Janmey, *Nature*, 2005, **435**, 191-194.
9. O. Chaudhuri, S. H. Parekh and D. A. Fletcher, *Nature*, 2007, **445**, 295-298.
10. C. P. Broedersz and F. C. MacKintosh, *Reviews of Modern Physics*, 2014, **86**, 995-1036.
11. F. Meng and E. M. Terentjev, *Polymers*, 2017, **9**, 52.
12. H. Hatami-Marbini and C. R. Picu, in *Advances in Soft Matter Mechanics*, Springer Berlin Heidelberg, Berlin, Heidelberg, 2012, DOI: 10.1007/978-3-642-19373-6_4, pp. 119-145.
13. J. Wilhelm and E. Frey, *Phys Rev Lett*, 2003, **91**, 108103.
14. D. A. Head, A. J. Levine and F. C. MacKintosh, *Phys Rev Lett*, 2003, **91**, 108102.
15. H. Hatami-Marbini and R. Picu, *Physical Review E*, 2008, **77**, 062103.
16. H. Hatami-Marbini, *Phys Rev E*, 2016, **93**, 042503.
17. H. Hatami-Marbini and R. C. Picu, *Phys Rev E*, 2009, **80**, 046703.
18. M. Rohanifar and H. Hatami-Marbini, *Mech Adv Mater Struc*, 2019, DOI: 10.1080/15376494.2018.1563251, 1-9.
19. M. Sheinman, C. Broedersz and F. MacKintosh, *Physical Review E*, 2012, **85**, 021801.
20. A. J. Licup, A. Sharma and F. C. MacKintosh, *Physical Review E*, 2016, **93**, 012407.
21. A. Sharma, A. J. Licup, R. Rens, M. Vahabi, K. A. Jansen, G. H. Koenderink and F. C. MacKintosh, *Phys Rev E*, 2016, **94**, 042407.

22. A. J. Licup, S. Münster, A. Sharma, M. Sheinman, L. M. Jawerth, B. Fabry, D. A. Weitz and F. C. MacKintosh, *Proc Natl Acad Sci USA*, 2015, **112**, 9573-9578.
23. T. Jin and I. Stanciulescu, *Biomech Model Mechanobiol*, 2016, **15**, 817-830.
24. G. Zagar, P. R. Onck and E. van der Giessen, *Biophys J*, 2015, **108**, 1470-1479.
25. D. Vader, A. Kabla, D. Weitz and L. Mahadevan, *PloS one*, 2009, **4**, e5902.
26. M. L. Gardel, J. H. Shin, F. C. MacKintosh, L. Mahadevan, P. Matsudaira and D. A. Weitz, *Science*, 2004, **304**, 1301-1305.
27. K. A. Erk, K. J. Henderson and K. R. Shull, *Biomacromolecules*, 2010, **11**, 1358-1363.
28. E. Ban, J. M. Franklin, S. Nam, L. R. Smith, H. Wang, R. G. Wells, O. Chaudhuri, J. T. Liphardt and V. B. Shenoy, *Biophysical Journal*, 2018, **114**, 450-461.
29. K. A. Jansen, A. J. Licup, A. Sharma, R. Rens, F. C. MacKintosh and G. H. Koenderink, *Biophys J*, 2018, **114**, 2665-2678.
30. H. Hatami-Marbini and V. Shriyan, *Phys Rev E*, 2017, **96**, 062502.
31. C. P. Broedersz, X. Mao, T. C. Lubensky and F. C. MacKintosh, *Nature Physics*, 2011, **7**, 983-988.
32. A. Kabla and L. Mahadevan, *Journal of the Royal Society Interface*, 2006, **4**, 99-106.
33. I. K. Piechocka, A. S. G. van Oosten, R. G. M. Breuls and G. H. Koenderink, *Biomacromolecules*, 2011, **12**, 2797-2805.
34. I. K. Piechocka, K. A. Jansen, C. P. Broedersz, N. A. Kurniawan, F. C. MacKintosh and G. H. Koenderink, *Soft matter*, 2016, **12**, 2145-2156.
35. S. B. Lindström, D. A. Vader, A. Kulachenko and D. A. Weitz, *Physical Review E*, 2010, **82**, 051905.
36. H. Hatami-Marbini, *Phys Rev E*, 2018, **97**, 022504.
37. J. A. J. van der Rijt, K. O. van der Werf, M. L. Bennink, P. J. Dijkstra and J. Feijen, *Macromol. Biosci.*, 2006, **6**, 697-702.
38. H. Hatami-Marbini and M. Rohanifar, *Journal of Engineering Mechanics*, 2020, **146**, 04019122.
39. H. Hatami-Marbini, *Philosophical Magazine Letters*, 2016, **96**, 165-174.
40. C. P. Broedersz and F. C. MacKintosh, *Soft Matter*, 2011, **7**, 3186-3191.
41. M. Wyart, H. Liang, A. Kabla and L. Mahadevan, *Physical Review Letters*, 2008, **101**, 215501.

42. L. Zhang, D. Z. Rocklin, L. M. Sander and X. Mao, *Physical Review Materials*, 2017, **1**, 052602.

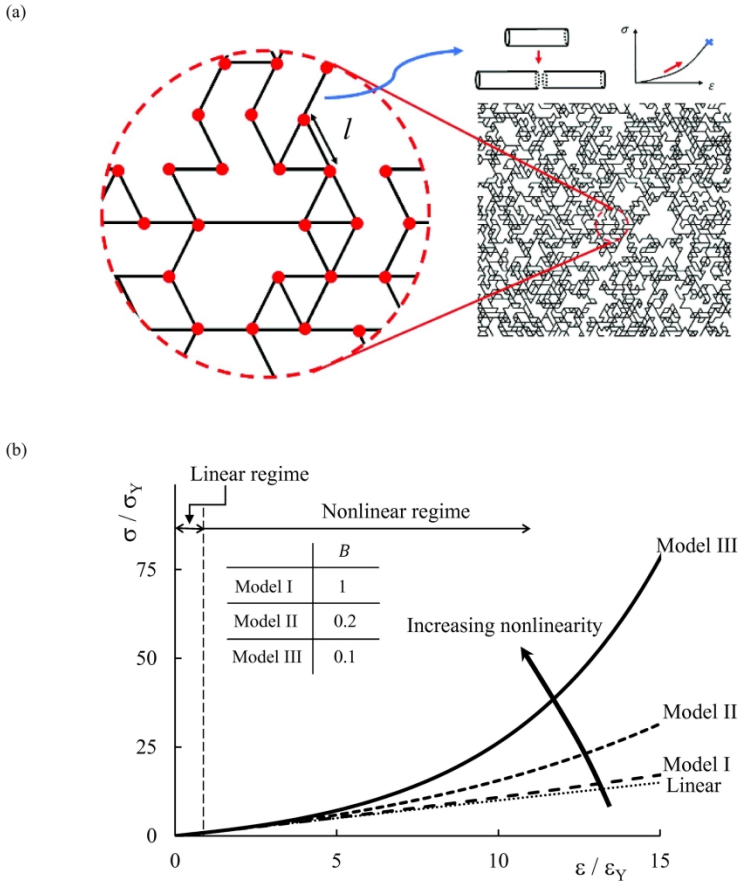


Figure 1. Please see the manuscript file for caption

215x279mm (300 x 300 DPI)

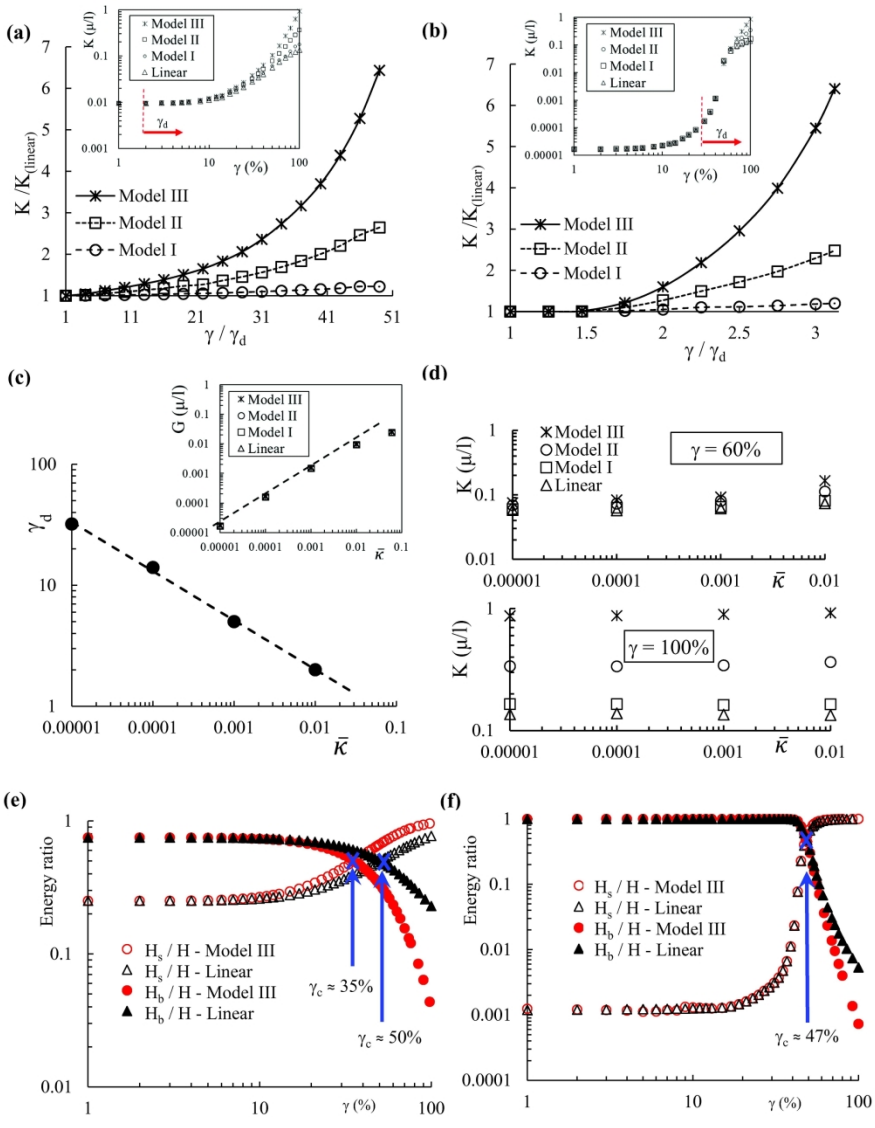


Figure 2. Please see the manuscript file for caption

215x279mm (300 x 300 DPI)

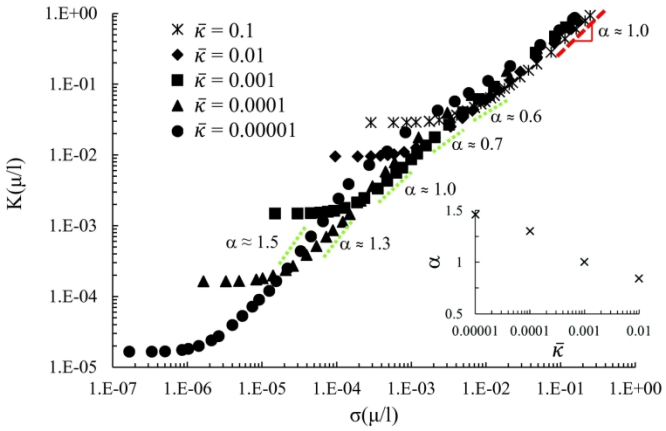


Figure 3. Please see the manuscript file for caption

215x279mm (300 x 300 DPI)

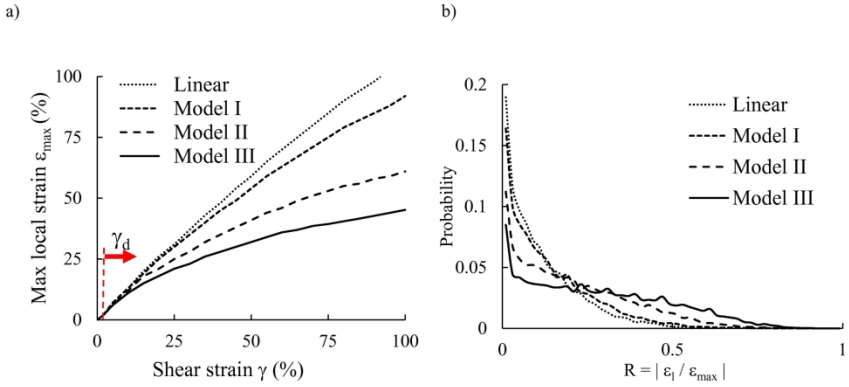


Figure 4. Please see the manuscript file for caption

215x279mm (300 x 300 DPI)

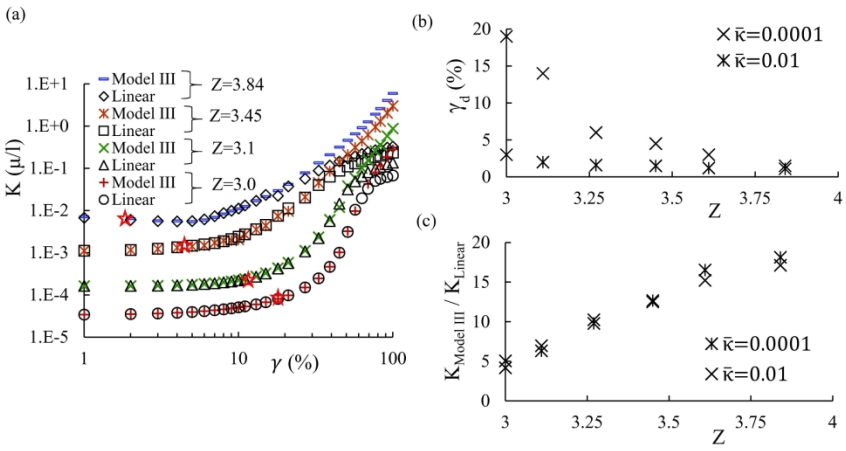


Figure 5. Please see the manuscript file for caption

215x279mm (300 x 300 DPI)

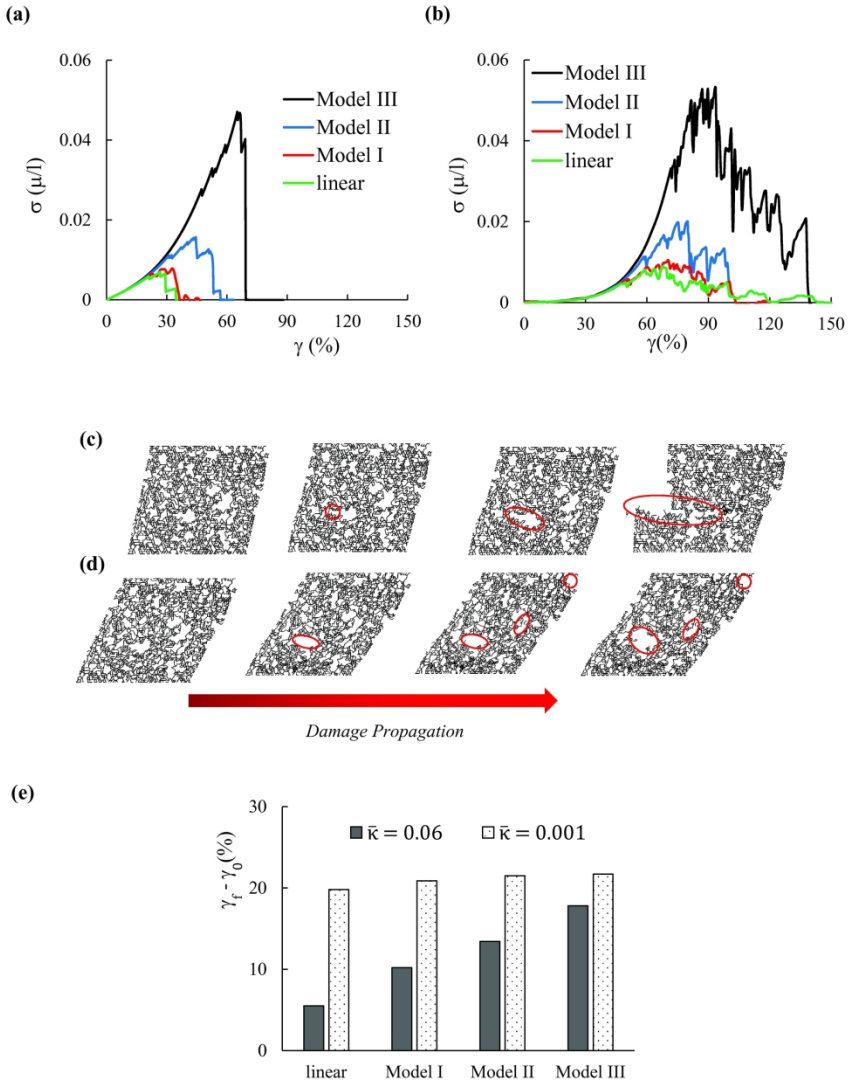


Figure 6. Please see the manuscript file for caption

215x279mm (300 x 300 DPI)

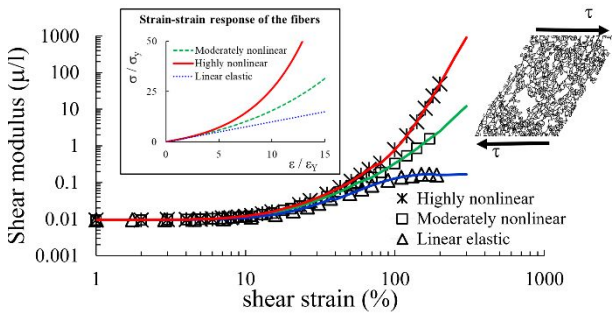


The effects of nonlinearity at the fiber level on the nonlinearity at the network level in subisostatic random network structures.